JACS
JOURNAL OF THE AMERICAN CHEMICAL SOCIETY

Communication

pubs.acs.org/JACS

New Powerful and Oxidatively Rugged Dinuclear Ru Water Oxidation Catalyst: Control of Mechanistic Pathways by Tailored Ligand Design

Sven Neudeck,[†] Somnath Maji,[‡] Isidoro López,[‡] Steffen Meyer,[†] Franc Meyer,*[,†] and Antoni Llobet*[,‡,§]

[†]Institute of Inorganic Chemistry, Georg-August-University Göttingen, D-37077 Göttingen, Germany

[‡]Institute of Chemical Research of Catalonia (ICIQ), E-43007 Tarragona, Spain

[§]Departament de Química, Universitat Autònoma de Barcelona, 08460 Cerdanyola del Vallès, Barcelona, Spain

Supporting Information

ABSTRACT: A new powerful and oxidatively rugged pyrazolate-based water oxidation catalyst of formula $\{[Ru^{II}(py\text{-}SO_3)_2(H_2O)]_2(\mu\text{-}Mebbp)\}^-$, $\mathbf{1}(H_2O)_2^-$, has been prepared and thoroughly characterized spectroscopically and electrochemically. This new catalyst has been conceived based on a specific ligand tailoring design, so that its performance has been systematically improved. It was also demonstrated how subtle ligand modifications cause a change in the O−O bond formation mechanism, thus revealing the close activation energy barriers associated with each pathway.

In order to come up with sustainable energy conversion schemes based on water splitting by sunlight,[1] a key step needs to be fully understood and controlled: the four electron oxidation of water to molecular oxygen (eq 1). This reaction is also of interest from a biological perspective since it is one of the crucial steps that occur in the oxygen evolving complex of photosystem II (OEC-PSII) in green plants and algae.[2] Therefore, the understanding of how water oxidation occurs on a molecular level is among the most important challenges faced by the scientific community today and by extension to our society that urgently needs an energy solution.[3]

$$2H_2O \rightarrow O_2 + 4H^+ + 4e^- \quad E^\circ = 1.23\text{V vs NHE at pH0} \qquad (1)$$

Important developments have taken place recently in the field of water oxidation catalysis (WOC) especially with regard to the discovery of a large body of molecular transition-metal complexes[4−6] with relatively large turnover numbers (TONs) and also with regard to catalytically active metal oxide materials.[7,8] Despite this progress, the mechanistic description of the different pathways under which these reactions proceed, together with the full spectroscopic characterization of reaction intermediates, is still a formidable challenge. We and others have contributed significantly toward this endeavor based on kinetics, UV−vis spectroscopy as well as ^{18}O labeling experiments.[9,10]

As in the case of the OEC-PSII in nature, transition-metal complexes and oxide materials aimed at catalyzing the water oxidation reaction have to comply with two conditions, namely the easy access to higher oxidation states via proton coupled electron transfer (PCET) and their capacity to make O−O bonds. For the former requirement, $M-OH_x$ type of complexes[11,12] are ideal and a large body of such complexes exists nowadays. With regard to the O−O bond formation step,

Scheme 1. Potential Metal-Mediated O−O Bond Formation Pathways for Ru=O Complexes

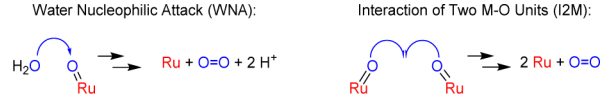

Chart 1. Ligands Used and Discussed in This Work

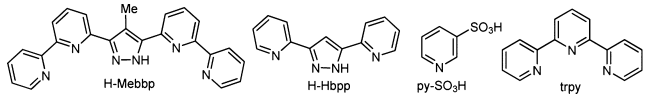

from a phenomenological viewpoint it can proceed via two different pathways, namely via a solvent water nucleophilic attack (WNA) or via an interaction of two M-O units (I2M) as depicted in Scheme 1 for the specific case of Ru=O complexes. In nature the actual way this takes place is still a subject of intense debate[2,13−15] but so far there is no final evidence in favor of WNA or I2M. With regard to synthetic transition-metal complexes many systems undergo WNA, while three examples have been reported to follow the I2M.[16,17] However, as has been put forward experimentally[10,18] and by DFT calculations,[9,19] there are occasions where the difference between the energy surfaces that drive the reaction to one mechanism or the other is relatively small. Thus it is of paramount importance to unravel and understand which ones are the crucial factors that govern the reactivity of the active intermediates.

We present an exceptional example of how subtle variations in ligand design can be used to regulate the O−O bond formation pathway, thus providing valuable information for the general conception of future WOCs. To that end, we report the synthesis, structure, spectroscopic, and electrochemical characterization of a new Ru dinuclear WOC, $\{[Ru^{II}(py\text{-}SO_3)_2(OH)]_2(\mu\text{-}Mebbp)\}^{3-}$, $\mathbf{1}(OH)_2^{3-}$, together with a detailed mechanistic description of the water oxidation reaction supported by ^{18}O labeling experiments.

The ligand $Mebbp^-$ (Chart 1) is a bis(tridentate) monoanionic ligand that has been designed to act as a bridging and compartmental scaffold placing two metal centers in close proximity. As such it has been previously used for the synthesis of [2 × 2] grid complexes which show interesting spin-crossover and redox properties.[20] Also shown in Chart 1 is $py\text{-}SO_3^-$ which

Received: September 27, 2013
Published: December 11, 2013

   dx.doi.org/10.1021/ja409974b | J. Am. Chem. Soc. 2014, 136, 24−27

Scheme 2. Synthetic Pathways and Molecular Structure of 2^{2+}

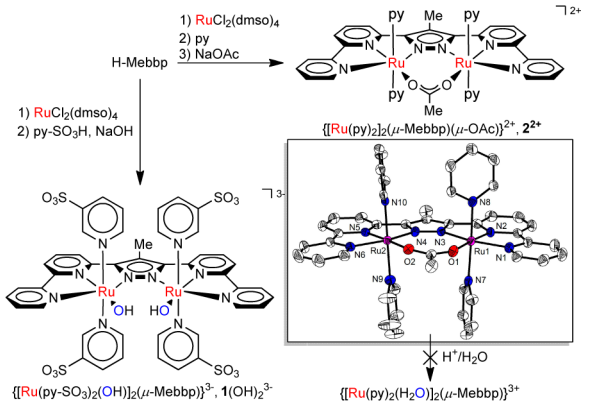

Chart 2. Complexes Discussed[4,9,25,26] in This Paper

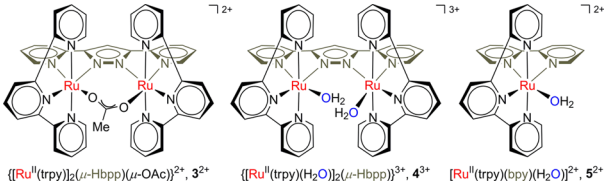

acts as a monodentate ligand; the sulfonate group helps overcoming the water solubility problems generally associated with many molecular WOCs. This is important because low water solubility prevents any proper spectroscopic and electrochemical characterization. It is even more important for the characterization of reaction mechanisms since the addition of an organic solvent such as MeCN can strongly enhance the degree of complexity of an already very complex reaction.

The synthesis of complex $\mathbf{1}(OH)_2^{3-}$, was achieved by reaction of H-Mebbp with 2 equiv of $[RuCl_2(dmso)_4]$. Addition of an excess of py-SO_3H in aqueous NaOH as indicated in Scheme 2 generated the desired dihydroxo complex in 22% yield. At pH = 1 the hydroxo ligands of $\mathbf{1}(OH)_2^{3-}$ are protonated giving the diaqua complex $\{[Ru^{II}(py\text{-}SO_3)_2(H_2O)]_2(\mu\text{-Mebbp})\}^-$, $\mathbf{1}(H_2O)_2^-$. In the same manner, but using pyridine instead of py-SO_3H and NaOAc in the last step instead of NaOH, the acetato bridged complex $\{[Ru^{II}(py)_2]_2(\mu\text{-Mebbp})(\mu\text{-OAc})\}^{2+}$, $\mathbf{2}^{2+}$, was also prepared. It is interesting to note that all attempts to use $\mathbf{2}^{2+}$ as starting material for the preparation of $\{[Ru^{II}(py)_2(H_2O)]_2(\mu\text{-Mebbp})\}^{3+}$ failed. This is in sharp contrast to the case of the related complex $\{[Ru^{II}(trpy)]_2(\mu\text{-Hbpp})(\mu\text{-OAc})\}^{2+}$, $\mathbf{3}^{2+}$ (trpy: 2,2′:6′,2″-terpyridine; Hbpp$^-$: 3,5-bis(2-pyridyl)pyrazolato dinucleating ligand, see Charts 1 and 2),[4] where simply dissolving $\mathbf{3}^{2+}$ in an aqueous pH 1 solution at RT instantaneously hydrolyzes the acetato bridge to generate the corresponding aqua complex $\{[Ru^{II}(trpy)(H_2O)]_2(\mu\text{-Hbpp})\}^{3+}$, $\mathbf{4}^{3+}$. The strikingly different reactivity is associated with a structural effect exerted by the Mebbp$^-$ ligand as described below.

Complexes $\mathbf{1}(OH)_2^{3-}$ and $\mathbf{2}^{2+}$ were structurally characterized in solution by NMR spectroscopy given the diamagnetic character of low-spin d^6 Ru(II) ions (see Figures S1−S12). Additionally complex $\mathbf{2}^{2+}$ was characterized in solid-state by X-ray crystallography (Scheme 2), which fully supports the structure deduced from NMR. The Mebbp$^-$ ligand in $\mathbf{2}^{2+}$ bridges both Ru centers and serves as a bis-meridional scaffold, and the monodentate pyridines occupy the axial positions. The acetato anion acts as a bridge between the two Ru metal centers. Bonding distances and angles are unremarkable for this type of complexes.[21] A noteworthy feature of this complex is the fact that all equatorial atoms from the Mebbp$^-$ and OAc$^-$ ligands are situated nearly within the equatorial plane, and as a consequence the RuNNRu torsion angle involving the two pyrazolate N atoms is only 0.4°. This strongly contrasts with the findings for the related complex $\mathbf{3}^{2+}$, where the same RuNNRu torsion angle is 25.4°.[4] In the latter case the distortion from an octahedral geometry is due to a balance between the crystal field stabilization energy for an octahedral geometry and the need to accommodate the acetate bridge in a *syn* fashion in a confined space. In the case of $\mathbf{2}^{2+}$, the constraints of the bis-tridentate bis-meridional ligand produce an enlargement of the Ru−Ru distance with regard to $\mathbf{3}^{2+}$, allowing the coordination of the acetate bridge in a very comfortable manner. As a result of this, the acetate bridge is very stable in $\mathbf{2}^{2+}$ and rather labile in $\mathbf{3}^{2+}$.

Cyclic voltammetry (CV) and square wave voltammetry (SWV) were used to electrochemically characterize complexes $\mathbf{1}(OH)_2^{3-}$ and $\mathbf{2}^{2+}$ at pH = 1.0. For $\mathbf{2}^{2+}$ two waves at 0.64 and 1.04 V vs SCE were observed as expected for this type of complexes (see Table 1 for assignment). The first potential is a bit lower for $\mathbf{2}^{2+}$ with respect to $\mathbf{3}^{2+}$, which can be ascribed to the small inductive effect exerted by the Me group of the Mebbp$^-$ ligand. The similarity of these redox potentials manifests a comparable electronic environment of the Ru metal centers both in terms of the electron density supplied by the donating atoms and also in terms of electronic coupling through the pyrazolato moiety. For the aqua complex $\mathbf{1}(H_2O)_2^-$ several waves can be observed, as depicted in Figure 1, whose assignment is presented in Table 1 together with the redox potential of $\mathbf{4}^{3+}$ and $[Ru(trpy)(bpy)(H_2O)]^{2+}$, $\mathbf{5}^{2+}$ (see Chart 2), for comparison purposes.

The assignment was further supported by redox titrations using Ce^{IV} at pH = 1.0 as an oxidant, which also allowed to spectroscopically characterize the different oxidation states. Further a Pourbaix diagram allowed elucidating the proton content of each species in the relevant pH range 0−1.5. Figure 2 shows the Pourbaix diagram and the UV−vis spectra at pH = 1.0 for the different oxidation states generated from $\mathbf{1}(H_2O)_2^-$, namely $[H_2O\text{−}Ru^{II}Ru^{II}\text{−}OH_2]^-$ (Mebbp$^-$ and py-SO_3^- ligands not written), $[HO\text{−}Ru^{III}Ru^{II}\text{−}OH_2]^-$, $[HO\text{−}Ru^{III}Ru^{III}\text{−}OH_2]$,

Table 1. Redox Potentials for $\mathbf{1}(H_2O)_2^-$ and $\mathbf{2}^{2+}$, Catalytic Data at pH = 1.0 for $\mathbf{1}(H_2O)_2^-$, and Data for Relevant Complexes

	$E_{1/2}$ [V vs SCE]							
complex	III,II/II,II	III,III/III,II	IV,III/III,III	IV,IV/IV,III	V,IV/IV,IV	TON (eff.)	TOF[a] [s^{-1}]	ref
$\mathbf{5}^{2+}$	0.79 (III/II)	0.98 (IV/III)	1.55 (V/IV)	–	–	18.3 (73.2%)	0.015	25, 26
$\mathbf{3}^{2+}$ (in DCM)[b]	0.72	1.04	–	–	–	–	–	4
$\mathbf{2}^{2+}$ (in PC)[c]	0.64	1.04	–	–	–	–	–	this work
$\mathbf{4}^{3+}$	0.58	0.64	0.87	1.09	–	17.5 (70.0%)	0.014	4, 9
$\mathbf{1}(H_2O)_2^-$	0.56	0.86	0.93	1.06	1.38	22.6 (90.4%)	0.068	this work

[a]Calculated TOF_i for a 1 mM catalyst and 100 mM Ce^{IV} experiment. [b]DCM: dichloromethane. [c]PC: propylene carbonate.

dx.doi.org/10.1021/ja409974b | J. Am. Chem. Soc. 2014, 136, 24−27

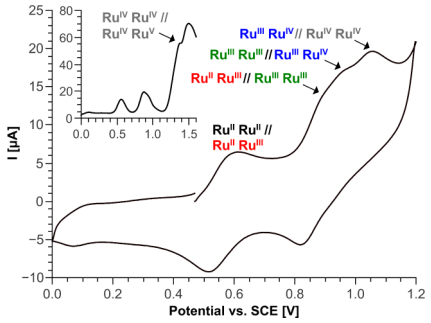

Figure 1. CV of $\mathbf{1}(H_2O)_2^-$ at pH 1.0 on a glassy carbon disk working electrode using Pt wire as an auxiliary and SCE as reference electrodes at a scan rate of 100 mV/s. Inset, SWV of $\mathbf{1}(H_2O)_2^-$ in the 0.0−1.6 V potential range.

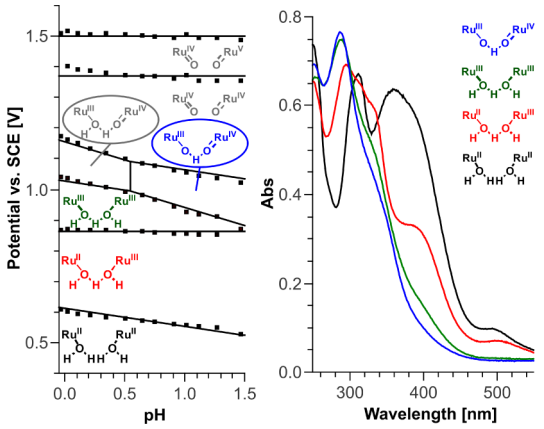

Figure 2. Pourbaix diagram (left) in the range of pH 0−1.5 of $\mathbf{1}(H_2O)_2^-$ in triflic acid solution and UV−vis spectrum (right) for $\mathbf{1}(H_2O)_2^-$ and three consecutively one-electron oxidized products at pH = 1.

and $[O-Ru^{IV}Ru^{III}-OH]^-$ that are generated chemically with well-behaved isosbestic points (see Figures S18−20). The spectra of the complex in oxidation state IV−IV, $[O-Ru^{IV}Ru^{IV}-O]^-$, could not be obtained due to the high reactivity of this species. As can be seen in Table 1, for $\mathbf{1}(H_2O)_2^-$ the potentials are different from those of $\mathbf{4}^{3+}$, as a consequence of the presence of the electron-withdrawing sulfonato groups and especially due to the different geometry imposed by the Mebbp$^-$ framework that changes significantly the degree of through space contacts of the Ru−OH_x units in $\mathbf{1}(H_2O)_2^-$. An interesting feature of complex $\mathbf{1}(H_2O)_2^-$, is the large anodic electrocatalytic wave in the 1.2−1.4 V range associated with the IV−V oxidation state and the generation of dioxygen. At 1.51 V another redox couple is observed in the SWV that is also pH independent in the 0−1.5 range. We propose this wave to be a further one electron oxidation of an intermediate that also leads to a catalytic process, since its proximity to the IV,IV−IV,V wave precludes a potential further one electron oxidation of the IV,V species.

Ce^{IV} was used as sacrificial oxidant in acidic pH in order to test the ability of complex $\mathbf{1}(H_2O)_2^-$ to act as catalyst for water oxidation. The system $\mathbf{1}(H_2O)_2^-$ (1 mM)/Ce^{IV} (100 mM) in 0.1 M triflic acid gave an impressive TON 22.6 of O_2 (90.4% efficiency with respect to oxidant) with an initial turnover frequency (TOF_i) of 0.068 Hz. The 1/1000 ($\mathbf{1}(H_2O)_2^-$/Ce(IV)) experiment gave TON 211 of O_2 practically maintaining the oxidative efficiency (84%), thus indicating the ruggedness of $\mathbf{1}(H_2O)_2^-$. Dioxygen measurements were simultaneously performed manometrically and with a Clarke electrode in the gas phase with very good agreement (see Figures S21−S22), thus confirming the absence any other gases. Under similar conditions complex $\mathbf{4}^{3+}$ gave a TON of 17.5 (70.0% efficiency). The improvement with regard to TON is associated with the protection of the pyrazole backbone with the Me group at C^4 that prevents its oxidation, as was reported to be a decomposition pathway for $\mathbf{4}^{3+}$.[9]

In addition the bis-facial nature of the Mebbp$^-$ ligand stabilizes the Ru−N coordination *trans* to the putative Ru^{IV}=O or Ru^{V}=O groups, by preventing rotation of the pyrazole ligands' pyridyl chelate arms and their potential substitution for an aqua ligand that would generate an undesired Ru *trans*-dioxo entity. The latter is known to be a dead end from a water oxidation catalysis perspective. This is important since as the oxidation state of the Ru−O entity increases the bond *trans* to it is significantly weakened. As a consequence, the elongated Ru−N bond can more easily suffer a substitution process in an irreversible manner, leading to a potential deactivation pathway. The improved geometrical design of the Mebbp$^-$ ligand prevents these deactivation pathways to occur and thus is responsible for the reactivity improvement.[22,23]

^{18}O labeling experiments are a valuable tool to obtain mechanistic information regarding the nature of the O−O bond formation step, provided that both catalyst and solvent have a different degree of ^{18}O labeling. For this purpose it is imperative that aqua ligand exchange is slow, since no mechanistic insight can be extracted in the case of fast exchange. We evaluated the substitution kinetics at different oxidation states using MeCN as a monodentate ligand in pseudo-first-order conditions yielding rate constant $k = 2.2 \times 10^{-3}$ s^{-1} for reaction 2,

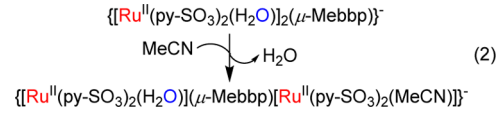

(2)

As the oxidation state increases the rate substantially decreases and for oxidation state III,III we obtained $k = 1.9 \times 10^{-5}$ s^{-1}, although deactivation reactions occur on a similar time scale (see Figures S23−25 and Table S1). This very slow substitution/deactivation kinetics enabled us carrying out ^{18}O labeling experiments with different degree of labeling at the catalyst and the solvent. Thus, our strategy consisted of dissolving complex $\mathbf{1}(H_2O)_2^-$ with a certain ratio of $H_2{}^{16}O/H_2{}^{18}O$ and allowing it to equilibrate. Subsequently, 2 equiv of Ce^{IV}, dissolved in water with the same degree of ^{18}O-labeling, generated the labeled catalysts at the III,III oxidation state. Further addition of 4 equiv of Ce^{IV} dissolved in water with a different degree of ^{18}O labeling generated, after a single turnover, dioxygen which was analyzed by online MS. Table 2 and Figure 3 report the isotopic analysis for the gases at the head space of the reactor following this strategy.

The experiments were done at different degrees of labeling, and in all cases they are consistent with an O−O bond formation reaction involving a WNA type of mechanism (see Figures S26−28 and Table S2). This is in sharp contrast with the Hbpp$^-$ analogue $\mathbf{4}^{3+}$ where the O−O bond formation takes place exclusively by an I2M mechanism. In $\mathbf{4}^{3+}$, as has been reported earlier,[24] there is a strong through space interaction of the two Ru−O groups. Thus, when the active Ru═O species are generated they immediately couple to make the O−O bond via an intramolecular I2M type of mechanism. For $\mathbf{1}(H_2O)_2^-$, as has been shown above, the constraints of the ligands produce a subtle

dx.doi.org/10.1021/ja409974b | J. Am. Chem. Soc. 2014, 136, 24−27

Table 2. Relative Isotopic Ratios of O_2 Evolved from the First Catalytic Cycle of $1(H_2O)_2^-$ at Different Degree of Catalyst and Solvent ^{18}O Labeling, Together with Expected Values Calculated for Different Reaction Mechanisms

$^{18}O^a$ (%)	O_2	exch.^{b}	WNA^c	I2M^d	expt
solv: 12.3	$^{32}O_2$	76.9	87.5	99.5	90.9
cat: 0.2	$^{34}O_2$	21.6	12.4	0.4	8.9
	$^{36}O_2$	1.5	2.3×10^4	4.2×10^4	0.2^e
	$^{32}O_2/^{34}O_2$	3.6	7.0	243.4	10.2
	$^{34}O_2/^{36}O_2$	14.3	493.9	973.6	37.1^e

^{a}Degree of solvent (solv.) and catalyst (cat.) ^{18}O labeling (%). ^{b}Expected ratios in the case of a fast O atom exchange. ^{c}Expected ratios for the WNA. ^{d}Expected ratios for an I2M mechanism. ^{e}Intensity of the $^{36}O_2$ trace is very low which leads to a large error.

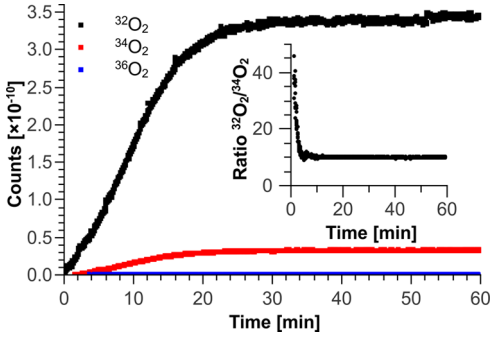

Figure 3. Online dioxygen evolution profiles monitored by MS upon addition of 4 equiv of Ce^{IV} dissolved in a 0.1 M triflic acid solution in 97.0% labeled $H_2{}^{18}O$, to a solution of $1(H_2O)_2^-$ at oxidation state III,III dissolved in 0.2% labeled $H_2{}^{18}O$ (final solution contains 0.2% ^{18}O labeled catalyst and 12.3% $H_2{}^{18}O$). Inset, $^{32}O_2/^{34}O_2$ ratio vs time.

change in geometry with regard to $\mathbf{4}^{3+}$, so that now the through space interaction of the two Ru−O groups is drastically reduced. For complex $\mathbf{4}^{3+}$ the ligand preorganization entropically highly favors the I2M mechanism, while this entropic term is basically lost in the case of $\mathbf{1}(H_2O)_2^-$; thus the preferred mechanism is now shifted to WNA.

In conclusion we report a new powerful and oxidatively rugged dinuclear Ru complex for which the different roles of the ligands have been carefully studied, understood, and tailored to improve catalyst performance. We also show that the Mebbp$^-$ ligand, if compared with Hbpp$^-$, induces subtle geometrical variations on the relative disposition of the active Ru−OH_x groups that regulate the O−O bond formation pathway and drive the mechanism toward the WNA. This demonstrates that the I2M and WNA pathways can have relatively close activation barriers, which constitutes a fundamental piece of information in the molecular water oxidation mechanistic landscape.

■ ASSOCIATED CONTENT

Supporting Information

Procedures and crystallographic data. This material is available free of charge via the Internet at http://pubs.acs.org.

■ AUTHOR INFORMATION

Corresponding Authors

allobet@iciq.es

franc.meyer@chemie.uni-goettingen.de

Notes

The authors declare no competing financial interest.

■ ACKNOWLEDGMENTS

Support from the international PhD program *Catalysis for Sustainable Synthesis* (*CaSuS*, fellowship for S.N.) as well as from the DFG (project Me 1313/9-1), MINECO (FPU grant for I.L.) ERA-Chem, and CTQ-2010-21497 are gratefully acknowledged.

■ REFERENCES

(1) Melis, A. *Energy Environ. Sci.* **2012**, *5*, 5531.
(2) Cox, N.; Pantazis, D. A.; Neese, F.; Lubitz, W. *Acc. Chem. Res.* **2013**, *46*, 1588.
(3) Styring, S. *Faraday Discuss.* **2012**, *155*, 357.
(4) Sens, C.; Romero, I.; Rodríguez, M.; Llobet, A.; Parella, T.; Benet-Buchholz, J. *J. Am. Chem. Soc.* **2004**, *126*, 7798.
(5) Sala, X.; Romero, I.; Rodriguez, M.; Escriche, L.; Llobet, A. *Angew. Chem. Int. Ed.* **2009**, *48*, 2842.
(6) Hetterscheid, D. G. H.; Reek, J. N. H. *Angew. Chem. Int. Ed.* **2012**, *51*, 9740.
(7) Osterloh, F. E. *Chem. Soc. Rev.* **2013**, *42*, 2294.
(8) Prevot, M. S.; Sivula, K. *J. Phys. Chem. C* **2013**, *117*, 17879.
(9) Bozoglian, F.; Romain, S.; Ertem, M. Z.; Todorova, T. K.; Sens, C.; Mola, J.; Rodriguez, M.; Romero, I.; Benet-Buchholz, J.; Fontrodona, X.; Cramer, C. J.; Gagliardi, L.; Llobet, A. *J. Am. Chem. Soc.* **2009**, *131*, 15176.
(10) Concepcion, J. J.; Tsai, M.-K.; Muckerman, J. T.; Meyer, T. J. *J. Am. Chem. Soc.* **2010**, *132*, 1545.
(11) Romain, S.; Vigara, L.; Llobet, A. *Acc. Chem. Res.* **2009**, *42*, 1944.
(12) Gagliardi, C. J.; Vannucci, A. K.; Concepcion, J. J.; Chen, Z.; Meyer, T. J. *Energy Environ. Sci.* **2012**, *5*, 7704.
(13) Sproviero, E. M.; Gascón, J. A.; McEvoy, J. P.; Brudvig, G. W.; Batista, V. S. *J. Am. Chem. Soc.* **2008**, *130*, 3428.
(14) Siegbahn, P. E. M. *Acc. Chem. Res.* **2009**, *42*, 1871.
(15) Rapatskiy, L.; Cox, N.; Savitsky, A.; Ames, W. M.; Sander, J.; Nowaczyk, M. M.; Rögner, M.; Boussac, A.; Neese, F.; Messinger, J.; Lubitz, W. *J. Am. Chem. Soc.* **2012**, *134*, 16619.
(16) Romain, S.; Bozoglian, F.; Sala, X.; Llobet, A. *J. Am. Chem. Soc.* **2009**, *131*, 2768.
(17) Maji, S.; Vigara, L.; Cottone, F.; Bozoglian, F.; Benet-Buchholz, J.; Llobet, A. *Angew. Chem., Int. Ed.* **2012**, *51*, 5967.
(18) Liu, F.; Concepcion, J. J.; Jurss, J. W.; Cardolaccia, T.; Templeton, J. L.; Meyer, T. J. *Inorg. Chem.* **2008**, *47*, 1727.
(19) Yang, X.; Baik, M.-H. *J. Am. Chem. Soc.* **2006**, *128*, 7476.
(20) (a) van der Vlugt, J. I.; Demeshko, S.; Dechert, S.; Meyer, F. *Inorg. Chem.* **2008**, *47*, 1576. (b) Schneider, B.; Demeshko, S.; Dechert, S.; Meyer, F. *Angew. Chem., Int. Ed.* **2010**, *49*, 9274. (c) Schneider, B.; Demeshko, S.; Neudeck, S.; Dechert, S.; Meyer, F. *Inorg. Chem.* **2013**, *52*, 13230.
(21) (a) Francas, L.; Sala, X.; Escudero-Adan, E.; Benet-Buchholz, J.; Escriche, L.; Llobet, A. *Inorg. Chem.* **2011**, *50*, 2771. (b) Planas, N.; Christian, G.; Roeser, S.; Mas-Marza, E.; Kollipara, M.-R.; Benet-Buchholz, J.; Maseras, F.; Llobet, A. *Inorg. Chem.* **2012**, *51*, 1889.
(22) Wasylenko, D. J.; Ganesamoorthy, C.; Koivisto, B. D.; Henderson, M. A.; Berlinguette, C. P. *Inorg. Chem.* **2010**, *49*, 2202.
(23) Planas, N.; Vigara, L.; Cady, C.; Miro, P.; Huang, P.; Hammarström, L.; Styring, S.; Leidel, N.; Dau, H.; Haumann, M.; Gagliardi, L.; Cramer, C.; Llobet, A. *Inorg. Chem.* **2011**, *50*, 11134.
(24) Planas, N.; Christian, G. J.; Mas-Marzá, E.; Sala, X.; Fontrodona, X.; Maseras, F.; Llobet, A. *Chem.—Eur. J.* **2010**, *16*, 7965.
(25) Wasylenko, D. J.; Ganesamoorthy, C.; Henderson, M. A.; Koivisto, B. D.; Osthoff, H. D.; Berlinguette, C. P. *J. Am. Chem. Soc.* **2010**, *132*, 16094.
(26) Maji, S.; López, I.; Bozoglian, F.; Benet-Buchholz, J.; Llobet, A. *Inorg. Chem.* **2013**, *52*, 3591.